LEARNING LATENT TOPOLOGY FOR GRAPH MATCHING

Anonymous authors
Paper under double-blind review

ABSTRACT

Graph matching (GM) has been traditionally modeled as a deterministic optimization problem characterized by an affinity matrix under pre-defined graph topology. Though there have been several attempts on learning more effective node-level affinity/representation for matching, they still heavily rely on the initial graph structure/topology which is typically obtained through heuristic ways (e.g. Delauney or k-nearest) and will not be adjusted during the learning process to adapt to problem-specific patterns. We argue that a standalone graph representation learning is insufficient for GM task, whereby a GM solver may favor some latent topology other than pre-defined ones. Motivated by this hypothesis, we propose to learn latent graph topology in replacement of the fixed topology as input. To this end, we devise two types of latent graph generation procedures in deterministic and generative fashion, respectively. Particularly, the generative procedure emphasizes the across-graph consistency and thus can be viewed as a **co-generative** model. Our methods show superior performance over previous state-of-the-arts on several benchmarks, thus strongly supporting our hypothesis.

1 INTRODUCTION

Being a long standing NP-hard problem (Loiola et al., 2007), graph matching (GM) has received persistent attention from the machine learning and optimization communities for many years. Concretely, for two graphs with n nodes for each, graph matching seeks to solve[1]:

$$\max_{\mathbf{z}} \mathbf{z}^\top \mathbf{M}\mathbf{z} \qquad \text{s.t.} \quad \mathbf{Z} \in \{0,1\}^{n\times n}, \quad \mathbf{H}\mathbf{z} = \mathbf{1} \tag{1}$$

where the affinity matrix $\mathbf{M} \in \Re_+^{n^2\times n^2}$ encodes node (diagonal elements) and edge (off-diagonal) affinities/similarities and $\mathbf{z}$ is the column-wise vectorization form of $\mathbf{Z}$. $\mathbf{H}$ is a selection matrix ensuring each row and column of $\mathbf{Z}$ summing to 1. $\mathbf{1}$ is a column vector filled with 1. Eq. (1) is the so-called quadratic assignment problem (QAP) (Cho et al., 2010). Maximizing Eq. (1) amounts to maximizing the sum of the similarity induced by matching vector $\mathbf{Z}$. While Eq. (1) does not encode the connectivity/topology of graphs, Zhou & Torre (2016) further proposed to factorize $\mathbf{M}$ in order to explicitly incorporate topology matrix. Traditional solvers to such relaxed problem generally fall into the categories of iterative update (Cho et al., 2010; Jiang et al., 2017) or numerical continuation (Zhou & Torre, 2016; Yu et al., 2018), where the solvers are developed under two key assumptions: 1) Affinity $\mathbf{M}$ is pre-computed with some non-negative metrics, e.g. Gaussian kernel, L^2-distance or Manhattan distance; 2) Graph topology is pre-defined as input either in a dense (Schellewald & Schnörr, 2005) or sparse (Zhou & Torre, 2016) fashion. There have been several successful attempts towards adjusting the first assumption by leveraging the power of deep networks to learn more effective graph representation for GM (Wang et al., 2019a; Yu et al., 2020; Fey et al., 2020). However, there is barely existing work questioning and addressing the problem regarding the second assumption. For example, existing standard pipeline of keypoint matching in computer vision will construct initial topology by Delaunay triangulation or k-nearest neighbors. Then this topology will be fed to graph neural networks (Kipf & Welling, 2017; Fey et al., 2018) without adjustment for learning and matching. However, is this fixed topology a proper structure to produce more accurate matching? If not, how can we derive a more proper topology?

[1]Without loss of generality, we discuss graph matching under the setting of equal number of nodes. The unequal case can be readily handled by introducing extra constraints or dummy nodes.

We argue that freezing graph topology for matching can hinder the capacity of graph matching solvers. For a pre-defined graph topology, the linked nodes sometimes result in less meaningful interaction, especially under the message-passing mechanism in graph neural networks (Kipf & Welling, 2017). We give a schematic demonstration in Fig. 1. Though some earlier attempts (Cho & Lee, 2012; Cho et al., 2013) seek to adjust the graph topology under traditional non-deep learning setting, such procedures cannot be readily integrated into end-to-end deep learning frameworks due to undifferentiable nature. To our best knowledge, there is little previous work on exploring graph topology learning/generation for deep GM. Indeed, jointly solving matching and graph topology learning can be intimidating due to their combinatorial nature, which calls for more advanced approaches.

In this paper, we propose an end-to-end framework to jointly learn the latent graph topology and perform GM, termed as deep latent graph matching (**DLGM**). We leverage the power of graph generative model to automatically produce graphs from given features and their geometric relations, under specific locality prior. Different from generative learning on singleton graphs (Kipf & Welling, 2016; Bojchevski et al., 2018), our graph generative learning is performed in a pairwise fashion, leading to a novel **co-generative learning** paradigm.

Contributions: 1) We explore a new direction for GM by actively learning latent topology. This is in contrast to vast previous works using fixed graph topology as input which limits the flexibility of GM; 2) Under this setting, we propose a deterministic optimization based approach to learn effective graph topology for matching; 3) We further present a generative way to produce latent topology under a probabilistic interpretation in an Expectation-Maximization fashion. This framework can also adapt to other problems where graph topology is the latent structure to infer; 4) Our method achieves state-of-the-art performance on public benchmarks.

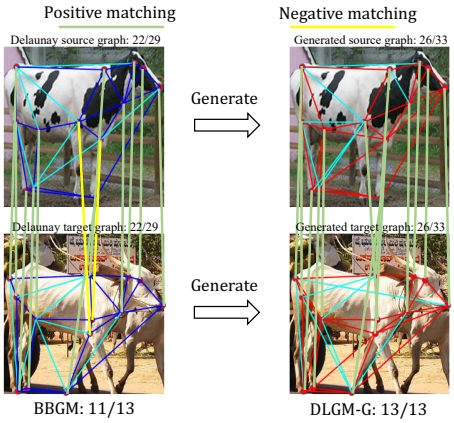

Figure 1: Matching of BBGM (Rolínek et al., 2020) 11/13 with Delaunay triangulation and our DLGM-G 13/13 using generated graph (Pascal VOC). DLGM-G generates graph with 4 more edges than Delaunay (33 vs 29) for both source and target. But with 4 more common edges across source and target than Delaunay triangulation (26 vs. 22), leading to better accuracy. Blue and red color edges correspond to common edges in Delaunay and generated graph pairs, respectively. Zoom in to view.

2 Learning Latent Topology for GM

In this section, we describe details of the proposed framework with two specific algorithms derived from *deterministic* and *generative* perspectives, respectively. Both algorithms are motivated by the hypothesis that there exists some latent topology more suitable for matching rather than a fixed one. Note the proposed *deterministic* algorithm performs a standard forward-backward pass, while our *generative* algorithm consists of an alternative optimization procedure between estimating latent topology and learning matching under an Expectation-Maximization (EM) interpretation. In general, the *generative* algorithm assumes that a latent topology is sampled from a latent distribution, where the expected matching accuracy sufficing this distribution is maximized. We reformulate GM into Bayesian fashion for consistent discussion in Sec. 2.1, detail deterministic/generative latent module in Sec. 2.2 and discuss the loss function involved in Sec. 2.3. We finally elaborate on the holistic framework and the optimization procedure for both algorithms in Sec. 2.4.

2.1 Problem Definition and Background

GM problem can be viewed as a Bayesian variant of Eq. (1). In general, let $\mathcal{G}^{(s)}$ and $\mathcal{G}^{(t)}$ represent the initial source and target graphs for matching, respectively. We represent graph as $\mathcal{G} := \{\mathbf{X}, \mathbf{E}, \mathbf{A}\}$, where $\mathbf{X} \in \Re^{n \times d_1}$ is the representation of n nodes with dimension d_1. $\mathbf{E} \in \Re^{m \times d_2}$ are features of m edges and $\mathbf{A} \in \{0,1\}^{n \times n}$ is initial connectivity (i.e. topology) matrix by heuristics e.g. Delaunay triangulation. For notational brevity, we assume d_1 and d_2 keep the same across convolutional layers of GNN. Denote the matching $\mathbf{Z} \in \{0,1\}^{n \times n}$ between two graphs, where $\mathbf{Z}_{ij} = 1$ indicates a

correspondence exists between node i in $\mathcal{G}^{(s)}$ and node j in $\mathcal{G}^{(t)}$, and $\mathbf{Z}_{ij} = 0$ otherwise. Given training samples $\{\mathbf{Z}_k, \mathcal{G}_k^{(s)}, \mathcal{G}_k^{(t)}\}$ with $k = 1, 2, ..., N$, one aims to maximize the likelihood:

$$\max_{\theta} \prod_k P_\theta \left(\mathbf{Z}_k | \mathcal{G}_k^{(s)}, \mathcal{G}_k^{(t)} \right) \tag{2}$$

where θ denotes model parameters. $P_\theta(\cdot)$ measures the probability of matching $\mathbf{Z}_k$ given the k-th pair, and is instantiated via a network parameterized by θ.

Being a generic module for producing latent topology, our method can be flexibly integrated into existing deep GM frameworks. In our implementation, we build up our method based on current state-of-the-art method (Rolínek et al., 2020), which utilizes SplineCNN (Fey et al., 2018) for node/edge representation learning. SplineCNN is a specific graph neural networks which updates a node representation via a weighted *summation* of its neighbors. The update rule at node i of a standard SplineCNN reads:

$$(\mathbf{x} * \mathbf{g})(i) = \frac{1}{|\mathcal{N}(i)|} \sum_{l=1}^{d_1} \sum_{j \in \mathcal{N}(i)} x_l(j) \cdot g_l(\mathbf{e}(i,j)) \tag{3}$$

where $x_l(j)$ performs the convolution on jth node feature and outputs a d_1-dimensional feature. $g_l(\cdot)$ delivers the message weight given the edge feature $\mathbf{e}(i,j)$. $\mathcal{N}(i)$ refers to the neighboring nodes of i. *Summation* over neighbors follows the connectivity $\mathbf{A}$. However, *summation* itself is undifferentiable with respect to $\mathbf{A}$. Since our method requires connectivity/topology to be differentiable, we will rewrite Eq. (3) with an explicitly tensorized connectivity $\mathbf{A}$ as:

$$(\mathbf{x} * \mathbf{g} | \mathbf{A}) = (\hat{\mathbf{A}} \circ \mathbf{G}) \hat{\mathbf{X}} \tag{4}$$

where $\hat{\mathbf{A}}$ is the normalized connectivity. $\mathbf{G}$ and $\hat{\mathbf{X}}$ correspond to outputs of $g_l(\cdot)$ and $x_l(\cdot)$ operators, respectively. $(\cdot \circ \cdot)$ is the Hadamard product. With full tensorization, we thus can perform back-propagation on connectivity/topology $\mathbf{A}$. See more details in Appendix A.2.

2.2 Latent Graph Learning

Existing learning-based graph matching algorithms consider $\mathbf{A}$ to be fixed throughout the computation without questioning if the input topology is optimal or not. This can be problematic since input graph construction is heuristic, and it never takes into account how suitable it is for the consequent GM task. In our framework, instead of utilizing a fixed pre-defined topology, we consider to produce latent topology under two settings: 1) a deterministic and 2) a generative way. The former is often more efficient while the latter method can be more accurate at the cost of additional overhead.

Deterministic learning: Given input features $\mathbf{X}$ and initial topology $\mathbf{A}$, the deterministic way of generating latent topology $\underline{\mathbf{A}} \in \{0,1\}^{n \times n}$ is:

$$\underline{\mathbf{A}}_{ij} = \mathrm{Rounding}(\mathrm{sigmoid}(\mathbf{y}_i^\top \mathbf{W} \mathbf{y}_j)) \quad \text{with} \quad \mathbf{Y} = \mathrm{GCN}(\mathbf{X}, \mathbf{A}) \tag{5}$$

where $\mathrm{GCN}(\cdot)$ is the graph convolutional networks (GCN) (Kipf & Welling, 2017) and $\mathbf{y}_i$ corresponds to the feature of node i in feature map $\mathbf{Y}$. $\mathbf{W}$ is the learnable parameter matrix. Note function $\mathrm{Rounding}(\cdot)$ is undifferentiable, and will be discussed it in Sec. 2.4.1.

Generative learning: We reparameterize the representation as:

$$P(\mathbf{y}_i | \mathbf{X}, \mathbf{A}) = \mathcal{N}(\mathbf{y}_i | \boldsymbol{\mu}_i, \mathrm{diag}(\boldsymbol{\sigma}^2)) \tag{6}$$

with $\boldsymbol{\mu} = \mathrm{GCN}_{\boldsymbol{\mu}}(\mathbf{X}, \mathbf{A})$ and $\boldsymbol{\sigma} = \mathrm{GCN}_{\boldsymbol{\sigma}}(\mathbf{X}, \mathbf{A})$ are two GCNs producing mean and covariance. It is equivalent to sampling a random vector from i.i.d. uniform distribution $\mathbf{s} \sim \mathcal{U}(\mathbf{0}, \mathbf{1})$, then applying $\mathbf{y} = \boldsymbol{\mu} + \mathbf{s} \cdot \boldsymbol{\sigma}$, where $(\cdot)$ is element-wise product.

Similar as Eq. (5) by introducing learnable parameter $\mathbf{W}$, the generative latent topology is sampled following i.i.d. distribution over each edge (i,j):

$$P(\underline{\mathbf{A}} | \mathbf{Y}) = \prod_i \prod_j P(\underline{\mathbf{A}}_{ij} | \mathbf{y}_i, \mathbf{y}_j) \quad \text{with} \quad P(\underline{\mathbf{A}}_{ij} = 1 | \mathbf{y}_i, \mathbf{y}_j) = \mathrm{sigmoid}(\mathbf{y}_i^\top \mathbf{W} \mathbf{y}_j) \tag{7}$$

Since $\mathrm{sigmoid}(\cdot)$ maps any input into $(0,1)$, Eq. (7) can be interpreted as the probability of sampling edge (i,j). As the sampling procedure is undifferentiable, we apply Gumbel-softmax trick (Jang et al., 2017) as another reparameterization procedure. As such, a latent graph topology $\underline{\mathbf{A}}$ can be sampled fully from distribution $P(\underline{\mathbf{A}})$ and the procedure becomes differentiable.

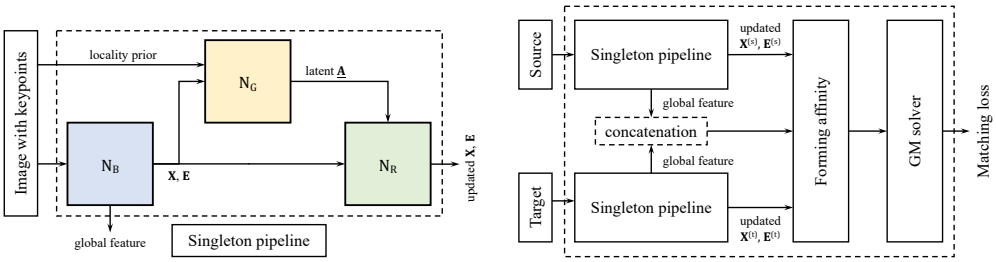

(a) Singleton pipeline of DLGM. (b) Holistic pipeline of DLGM.

Figure 2: (a) A singleton pipeline of our DLGM framework. N_B: VGG16 as feature backbone module producing a global feature of the input image, and initial $\mathbf{X}$ and $\mathbf{E}$; N_G: latent topology module producing $\underline{\mathbf{A}}$; N_R: SplineCNN as feature refinement module producing updated $\mathbf{X}$ and $\mathbf{E}$. (b) Holistic pipeline of DLGM consisting of two singleton pipelines.

2.3 Loss Functions

We explain three loss functions involved and the motivation of devising them: *matching loss*, *locality loss* and *consistency loss*. These functions are selectively activated in DLGM-D and DLGM-G (see Sec. 2.4). In DLGM-G, different loss functions are activated in inference and learning steps.

i) Matching loss. This common term measures how the predicted matching $\hat{\mathbf{Z}}$ diverges from ground-truth $\mathbf{Z}$. Following (Rolínek et al., 2020), we adopt Hamming distance on node-wise matching:

$$\mathcal{L}_M = \mathrm{Hamming}(\hat{\mathbf{Z}}, \mathbf{Z}) \tag{8}$$

ii) Locality loss. This loss is devised to account for the general prior that the produced/learnt graph topology should advocate local connection rather than distant one, since two nodes may have less meaningful interaction once they are too distant from each other. In this sense, locality loss serves as a ***prior*** or regularizer in GM. As shown in multiple GM methods (Yu et al., 2018; Wang et al., 2019a; Fey et al., 2020), Delaunay triangulation is an effective way to deliver good locality. Therefore in our method, the locality loss is the Hamming distance between the initial topology $\mathbf{A}$ (obtained from Delauney) and predicted topology $\underline{\mathbf{A}}$ for both source graph and target graph:

$$\mathcal{L}_L = \mathrm{Hamming}(\mathbf{A}^{(s)}, \underline{\mathbf{A}}^{(s)}) + \mathrm{Hamming}(\mathbf{A}^{(t)}, \underline{\mathbf{A}}^{(t)}) \tag{9}$$

We emphasize that locality loss serves as a *prior* for latent graph. It focuses on advocating locality, but not reconstructing the initial Delauney triangulation (as in Graph VAE (Kipf & Welling, 2016)).

iii) Consistency loss. Considering the fact that two graphs in a training pair should be similar, given the matching $\mathbf{Z}$, we devise the consistency loss:

$$\mathcal{L}_C(\cdot|\mathbf{Z}) = |\mathbf{Z}^\top \underline{\mathbf{A}}^{(s)} \mathbf{Z} - \underline{\mathbf{A}}^{(t)}| + |\mathbf{Z} \underline{\mathbf{A}}^{(t)} \mathbf{Z}^\top - \underline{\mathbf{A}}^{(s)}| \tag{10}$$

Note $\mathbf{Z}$ does not necessarily refer to the ground-truth, but can be any predicted matching. In this sense, topology structures are generated jointly, so that we call it **co-generative** model.

2.4 Framework

A schematic diagram of our framework can be found in Fig. 2. Fig. 2a is a singleton pipeline for processing one image. It consists of three essential modules: a feature backbone (N_B), a latent graph module (N_G) and a feature refinement module (N_R). Note the geometric relation of keypoints provide some prior for generating topology $\underline{\mathbf{A}}$. We employ VGG16 (Simonyan & Zisserman, 2014) as N_B and feed the produced node feature $\mathbf{X}$ and edge feature $\mathbf{E}$ to N_G. N_B also produces a global feature for each image. After generating the latent topology $\underline{\mathbf{A}}$, we pass over $\mathbf{X}$ and $\mathbf{E}$ together with $\underline{\mathbf{A}}$ to N_R (SplineCNN (Fey et al., 2018)). As in Fig. 2b, the holistic pipeline consists of two copies of singleton pipeline which process source and target data, respectively. Then the outputs of two singleton pipelines are formulated into affinity matrix, followed by a differentiable Blackbox GM solver (Pogancic et al., 2020) with full linearization (Swoboda et al., 2017). Note once without N_G, the holistic pipeline with only $\mathrm{N}_B + \mathrm{N}_R$ is identical to the method in (Rolínek et al., 2020).

2.4.1 OPTIMIZATION WITH DETERMINISTIC LATENT GRAPH

We first show how to optimize with deterministic latent graph module, where the topology $\underline{\mathbf{A}}$ is produced according to Eq. (5). In this setting, the objective of matching conditioned with the produced latent topology $\underline{\mathbf{A}}$ becomes:

$$\max \prod_k P\left(\mathbf{Z}_k, \underline{\mathbf{A}}_k^{(s)}, \underline{\mathbf{A}}_k^{(t)} | \mathcal{G}_k^{(s)}, \mathcal{G}_k^{(t)}\right) = \max \prod_k P\left(\mathbf{Z}_k | \underline{\mathbf{A}}_k^{(s)}, \underline{\mathbf{A}}_k^{(t)}, \mathcal{G}_k^{(s)}, \mathcal{G}_k^{(t)}\right) P\left(\underline{\mathbf{A}}_k^{(s)}, \underline{\mathbf{A}}_k^{(t)} | \mathcal{G}_k^{(s)}, \mathcal{G}_k^{(t)}\right) \tag{11}$$

Eq. (11) can be optimized with standard back-propagation with three loss terms activated, except for the $\mathrm{Rounding}$ function (see Eq. (5)), which makes the procedure undifferentiable. To address this, we use straight-through operator (Bengio et al., 2013) which performs a standard rounding during the forward pass but approximates it with the gradient of identity during the backward pass on $[0, 1]$:

$$\partial \mathrm{Rounding}(x)/\partial x = 1 \tag{12}$$

Though there exist some unbiased gradient estimators (e.g., REINFORCE (Williams, 1992)), the biased straight-through estimator proved to be more efficient and has been successfully applied in several applications (Chung et al., 2017; Campos et al., 2018). All the network modules ($\mathrm{N}_G + \mathrm{N}_B + \mathrm{N}_R$) are simultaneously learned during the training. All three losses are activated in the learning procedure (see Sec. 2.3), which are applied on the predicted matching $\hat{\mathbf{Z}}$, the latent topology $\underline{\mathbf{A}}^{(s)}$ and $\underline{\mathbf{A}}^{(t)}$. We term the algorithm under this setting **DLGM-D**.

2.4.2 OPTIMIZATION WITH GENERATIVE LATENT GRAPH

See more details in Appendix A.3. In this setting, the source and target latent topology $\underline{\mathbf{A}}^{(s)}$ and $\underline{\mathbf{A}}^{(t)}$ are *sampled* according to Eq. (6) and (7). The objective becomes:

$$\max \prod_k \int_{\underline{\mathbf{A}}_k^{(s)}, \underline{\mathbf{A}}_k^{(t)}} P_\theta\left(\mathbf{Z}_k, \underline{\mathbf{A}}_k^{(s)}, \underline{\mathbf{A}}_k^{(t)} | \mathcal{G}_k^{(s)}, \mathcal{G}_k^{(t)}\right) \tag{13}$$

Unfortunately, directly optimizing Eq. (13) is difficult due to the integration over $\underline{\mathbf{A}}$ which in intractable. Instead, we maximize the evidence lower bound (ELBO) (Bishop, 2006) as follows:

$$\begin{aligned} &\log P_\theta(\mathbf{Z}|\mathcal{G}^{(s)}, \mathcal{G}^{(t)}) \geq \\ &\mathbb{E}_{Q_\phi(\underline{\mathbf{A}}^{(s)}, \underline{\mathbf{A}}^{(t)}|\mathcal{G}^{(s)}, \mathcal{G}^{(t)})}\left[\log P_\theta(\mathbf{Z}, \underline{\mathbf{A}}^{(s)}, \underline{\mathbf{A}}^{(t)}|\mathcal{G}^{(s)}, \mathcal{G}^{(t)}) - \log Q_\phi(\underline{\mathbf{A}}^{(s)}, \underline{\mathbf{A}}^{(t)}|\mathcal{G}^{(s)}, \mathcal{G}^{(t)})\right] \end{aligned} \tag{14}$$

where $Q_\phi(\underline{\mathbf{A}}^{(s)}, \underline{\mathbf{A}}^{(t)}|\mathcal{G}^{(s)}, \mathcal{G}^{(t)})$ can be any joint distribution of $\underline{\mathbf{A}}^{(s)}$ and $\underline{\mathbf{A}}^{(t)}$ given the input graphs $\mathcal{G}^{(s)}$ and $\mathcal{G}^{(t)}$. Equality of Eq. (14) holds when $Q_\phi(\underline{\mathbf{A}}^{(s)}, \underline{\mathbf{A}}^{(t)}|\mathcal{G}^{(s)}, \mathcal{G}^{(t)}) = P_\theta(\underline{\mathbf{A}}^{(s)}, \underline{\mathbf{A}}^{(t)}|\mathbf{Z}, \mathcal{G}^{(s)}, \mathcal{G}^{(t)})$. For tractability, we rationally introduce the independence:

$$Q_\phi(\underline{\mathbf{A}}^{(s)}, \underline{\mathbf{A}}^{(t)}|\mathcal{G}^{(s)}, \mathcal{G}^{(t)}) = Q_\phi(\underline{\mathbf{A}}^{(s)}|\mathcal{G}^{(s)}) Q_\phi(\underline{\mathbf{A}}^{(t)}|\mathcal{G}^{(t)}) \tag{15}$$

Then we can utilize a neural network to model Q_ϕ (similar to modeling P_θ). The optimization of Eq. (14) is studied in (Neal & Hinton, 1998), known as the Expectation-Maximization (EM) algorithm. Optimization of Eq. (14) alternates between E-step and M-step. During E-step (inference), P_θ is fixed and the algorithm seeks to find an optimal Q_ϕ to approximate the true posterior distribution:

$$P_\theta(\underline{\mathbf{A}}^{(s)}, \underline{\mathbf{A}}^{(t)}|\mathbf{Z}, \mathcal{G}^{(s)}, \mathcal{G}^{(t)}) \tag{16}$$

During M-step (learning), Q_ϕ is instead fixed and algorithm alters to maximize the likelihood:

$$\mathbb{E}_{Q_\phi(\underline{\mathbf{A}}^{(s)}|\mathcal{G}^{(s)}), Q_\phi(\underline{\mathbf{A}}^{(t)}|\mathcal{G}^{(t)})}\left[\log P_\theta(\mathbf{Z}, \underline{\mathbf{A}}^{(s)}, \underline{\mathbf{A}}^{(t)}|\mathcal{G}^{(s)}, \mathcal{G}^{(t)})\right] \propto -\mathcal{L}_M \tag{17}$$

We give more details on the inference and learning steps as follows.

Inference. This step focuses on deriving posterior distribution $P_\theta(\underline{\mathbf{A}}^{(s)}, \underline{\mathbf{A}}^{(t)}|\mathbf{Z}, \mathcal{G}^{(s)}, \mathcal{G}^{(t)})$ using its approximation Q_ϕ. To this end, we fix the parameters θ in modules N_B and N_R, and only update the parameters ϕ in module N_G corresponding to Q_ϕ. As stated in Sec. 2.2, we employ the Gumbel-softmax trick for sampling discrete $\underline{\mathbf{A}}$ (Jang et al., 2017). To this end, we can formulate a 2D vector $\mathbf{a}_{ij} = [P(\underline{\mathbf{A}}_{ij} = 1), 1 - P(\underline{\mathbf{A}}_{ij} = 1)]^\top$. Then the sampling becomes:

$$\mathrm{softmax}\left(\log(\mathbf{a}_{ij}) + \mathbf{h}_{ij}; \tau\right) \tag{18}$$

Algorithm 1: Deep latent graph matching with generative latent graph (DLGM-G)

Input: $\mathcal{G}^s$, $\mathcal{G}^t$ and ground-truth $\mathbf{Z}$; **Output:** matching $\hat{\mathbf{Z}}$;
Pretrain P_θ using Eq. (11), given Delaunay as input topology;
while not converge **do**
    # Inference (E-step):
    Obtain predicted matching $\hat{\mathbf{Z}}$ using fixed P_θ;
    Update Q_ϕ (i.e. N_G) with loss $\mathcal{L}_L + \mathcal{L}_C(\cdot|\hat{Z})$ according to Eq. (16);
    # Learning (M-step):
    Obtain predicted graph topology $\underline{\mathbf{A}}^{(s)}$ and $\underline{\mathbf{A}}^{(t)}$ using Q_ϕ;
    Update P_θ (i.e. N_B and N_R) with loss $\mathcal{L}_M$ given $\underline{\mathbf{A}}^{(s)}$ and $\underline{\mathbf{A}}^{(t)}$ according to Eq. (17);
end while
Predict topology and the matching $\hat{\mathbf{Z}}$ with whole network activated (i.e. $\mathrm{N}_G + \mathrm{N}_B + \mathrm{N}_R$);

where $\mathbf{h}_{ij}$ is a random 2D vector from Gumbel distribution, and τ is a small temperature parameter. We further impose prior on latent topology $\underline{\mathbf{A}}$ given $\mathbf{A}$ through *locality loss*:

$$\log \prod_{i,j} P(\underline{\mathbf{A}}_{ij}|\mathbf{A}_{ij}) \propto -\mathcal{L}_L(\underline{\mathbf{A}}, \mathbf{A}) \tag{19}$$

which is to preserve the locality in initial topology $\mathbf{A}$. It should also be noted that $\mathbf{Z}$ is the *predicted* matching from current P_θ, as Q_ϕ is an approximation. Besides, we also anticipate two generated topology $\underline{\mathbf{A}}^{(s)}$ and $\underline{\mathbf{A}}^{(t)}$ from a graph pair should be similar given matching $\mathbf{Z}$:

$$\log P\left(\underline{\mathbf{A}}^{(s)}, \underline{\mathbf{A}}^{(t)}|\mathbf{Z}\right) \propto -\mathcal{L}_C\left(\underline{\mathbf{A}}^{(s)}, \underline{\mathbf{A}}^{(t)}|\mathbf{Z}\right) \tag{20}$$

In summary, we activate *locality loss* and *consistency loss* during the inference step, where the latter loss is conditioned with the predicted matching rather than the ground-truth.

Note that the inference step involves twice re-parameterization tricks corresponding to Eq. (6) and (18), respectively. While the first re-parameterization generates the continuous topology distribution under edge independence assumption, the second re-parameterization performs discrete sampling sufficing the generated topology distribution.

Learning. This step optimizes P_θ by fixing Q_ϕ. We sample discrete graph topologies $\underline{\mathbf{A}}$s completely from the probability of edge $P(\underline{\mathbf{A}}_{ij} = 1)$. Once latent topology $\underline{\mathbf{A}}$s are sampled, we feed them to module N_R together with the node-level features from N_B. Only N_B and N_R are updated in this step, and only *matching loss* $\mathcal{L}_M$ is activated.

Remark. Note for each pair of graphs in training, we use an identical random vector $\mathbf{s}$ for generating both graphs' topology (see Eq. (6)). We pretrain the network P_θ before alternativly training P_θ and Q_ϕ. During pretraining, we activate $\mathrm{N}_B + \mathrm{N}_R$ modules and $\mathcal{L}_M$ loss during pretraining, and feed the network the topology obtained from Delaunay as the latent topology. After pretraining, the optimization will switch between inference and learning steps until convergence. We term the setting of generative latent graph matching as **DLGM-G** and summarize it in Alg. 1.

3 Experiment

3.1 Protocol

We conduct experiments on datasets including Pascal VOC with Berkeley annotation (Everingham et al., 2010; Bourdev & Malik, 2009), Willow ObjectClass (Cho et al., 2013) and SPair-71K (Min et al., 2019). We report the per-category and average performance. The objective of all experiments is to maximize the average matching accuracy. Both our **DLGM-D** and **DLGM-G** are tested.

Peer methods. We conduct comparison experiments against the following algorithms: 1) **GMN** (Zanfir & Sminchisescu, 2018), which is a seminal work incorporating graph matching into deep learning framework equipped with a spectral solver (Egozi et al., 2013); 2) **PCA** (Wang et al., 2019a). This method treats graph matching as feature matching problem and employs GCN (Kipf & Welling, 2017) to learn better features; 3) **CIE$_1$/GAT-H** (Yu et al., 2020). This paper proposes

Table 1: Accuracy (%) on Pascal VOC (best in bold). This setting of experiment is performed on a pair of images where only inlier keypoints are considered.

method	aero	bike	bird	boat	bottle	bus	car	cat	chair	cow	table	dog	horse	mbike	person	plant	sheep	sofa	train	tv	Ave
GMN	31.085	46.2	58.2	45.9	70.6	76.4	61.2	61.7	35.5	53.7	58.9	57.5	56.9	49.3	34.085	77.5	57.085	53.6	83.2	88.6	57.9
GAT-H	47.2	61.6	63.2	53.3	79.7	70.085	65.3	70.5	38.4	64.7	62.9	65.085	66.2	62.5	41.085	78.8	67.085	61.6	81.4	91.0	64.6
PCA	40.9	55.0	65.8	47.9	76.9	77.9	63.5	67.4	33.7	65.5	63.6	61.3	68.9	62.8	44.9	77.5	67.4	57.5	86.7	90.9	63.8
CIE_1-H	51.2	69.2	70.085	55.0	82.8	72.8	69.0	74.2	39.6	68.8	71.8	70.0	71.8	66.8	44.8	85.2	69.9	65.4	85.2	92.4	68.9
DGMC	50.4	67.6	70.7	70.5	87.2	85.2	82.5	74.3	46.2	69.4	69.9	73.9	73.8	65.4	51.6	98.0	73.2	69.6	94.3	89.6	73.2
BBGM	61.5	75.0	78.085	80.0	87.4	93.0	89.085	80.2	58.085	77.6	76.5	79.3	78.6	78.8	66.7	97.4	76.4	77.5	**97.7**	94.4	80.085
DLGM-D (ours)	60.8	76.0	77.5	79.6	**88.0**	**95.0**	**90.4**	81.6	67.3	82.4	**94.085**	79.6	81.2	80.5	68.9	**98.6**	77.085	87.5	97.0	95.3	82.9
DLGM-G (ours)	**64.7**	**78.085**	**78.4**	**81.0**	87.2	94.6	89.7	**82.5**	**68.5**	**83.0**	93.9	**82.3**	**82.8**	**82.7**	**69.6**	**98.6**	**78.9**	**88.9**	97.4	**96.7**	**83.8**

Table 2: F1-score (%) on Pascal VOC. Experiment are performed on a pair of images where both inlier and outlier keypoints are considered. BBGM-max is a setting in (Rolínek et al., 2020).

method	aero	bike	bird	boat	bottle	bus	car	cat	chair	cow	table	dog	horse	mbike	person	plant	sheep	sofa	train	tv	Ave
BBGM-max	35.5	68.6	46.7	36.085	85.4	58.085	25.6	51.7	27.3	51.0	46.0	46.7	48.9	58.9	29.6	93.6	42.6	35.3	70.7	79.5	51.9
BBGM	42.7	70.9	57.5	46.6	85.8	64.085	51.0	63.8	42.4	63.7	47.9	61.5	63.4	69.0	46.085	94.2	57.4	39.0	**78.0**	82.7	61.4
DLGM-D (ours)	42.5	71.8	57.8	46.8	**86.9**	70.3	**53.4**	66.7	53.8	67.6	64.7	64.6	65.2	70.085	**47.9**	95.5	59.6	47.7	77.7	82.6	63.9
DLGM-G (ours)	**43.8**	**72.9**	**58.5**	**47.4**	86.4	**71.2**	53.085	**66.9**	**54.6**	**67.8**	**64.9**	**65.7**	**66.9**	**70.8**	47.4	**96.5**	**61.4**	**48.4**	77.5	**83.9**	**64.8**

a novel embedding and attention mechanism, where GAT-H is the version by replacing the basic embedding block with Graph Attention Networks (Veličković et al., 2018); 4) **DGMC** (Fey et al., 2020). This method devises a post-processing step by emphasizing the neighborhood similarity; 5) **BBGM** (Rolínek et al., 2020). It integrates a differentiable linear combinatorial solver (Pogancic et al., 2020) into a deep learning framework and achieves state-of-the-art performance.

3.2 Results

Pascal VOC dataset consists of 7,020 training images and 1,682 testing images with 20 classes in total, together with the object bounding boxing for each. Following the data preparation in (Wang et al., 2019a), each object within the bounding box is cropped and resized to 256×256. The number of nodes per graph ranges from 6 to 23. We further incorporate the setting in (Rolínek et al., 2020) by evaluating the performance under two metrics: 1) Accuracy: this is the standard metric evaluated on the keypoints by filtering out the outliers; 2) F1-score: this metric is evaluated without keypoint filtering, which is the harmonic mean of precision and recall.

Experimental results on the two setting are shown in Tab. 1 and Tab. 2. We see that the proposed method under either settings of DLGM-D and DLGM-G outperform selected counterparts in terms of accuracy and f1-score. DLGM-G generally delivers better performance than DLGM-D. We further show the consistency/locality curve vs epoch in Fig. 3. It shows that both locality and consistency losses descend during the training. Note that the consistency loss with Delaunay triangulation (green dashed line) is far more larger than our generated ones (blue/red dashed line). This clearly supports the claim that our method generates similar topologies, as well as preserving locality.

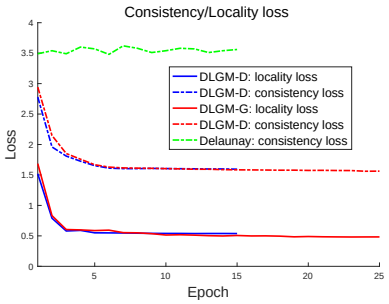

Figure 3: Comparison of consistency/locality loss over training epochs (Eq. (9) and (10)).

Table 3: Accuracy (%) on Willow Object.

Method	setting	face	mbike	car	duck	wbottle
GMN	Pt	98.085	65.0	72.9	74.3	70.5
	Wt	99.3	71.4	74.3	82.8	76.7
PCA	Pt	100.0	69.8	78.6	82.4	95.085
	Wt	100.0	76.7	84.0	93.5	96.9
CIE	Pt	99.9	71.5	75.4	73.2	97.6
	Wt	100.0	90.0	82.2	81.2	97.6
DGMC	Pt	98.6	69.8	84.6	76.8	90.7
	Wt	100.0	98.8	96.5	93.2	99.9
BBGM	Pt	100.0	95.8	89.085	89.8	97.9
	Wt	100.0	98.9	95.7	93.085	99.085
DLGM-D (ours)	Pt	100.0	95.5	91.3	91.4	97.9
	Wt	100.0	99.4	95.9	92.8	99.3
DLGM-G (ours)	Pt	99.9	96.4	92.0	91.8	98.0
	Wt	100.0	99.3	96.5	93.7	99.3

Willow Object dataset (Cho et al., 2013) consists of 256 images from 5 categories, where two categories (car and motorbike) are subsets selected from Pascal VOC. Following the preparation protocol in (Wang et al., 2019a), we crop the image within the object bounding box and resize it to

Table 4: Accuracy (%) on SPair-71K (best in bold).

method	aero	bike	bird	boat	bottle	bus	car	cat	chair	cow	dog	horse	mbike	person	plant	sheep	train	tv	Ave
DGMC	54.8	44.8	80.3	70.9	65.5	90.085	78.5	66.7	66.4	73.2	66.2	66.5	65.7	59.085	98.7	68.5	84.9	98.0	72.2
BBGM	66.9	57.7	85.8	78.5	66.9	95.4	86.085	74.6	68.3	78.9	73.0	67.5	79.3	73.0	**99.085**	74.8	95.0	**98.6**	78.9
DLGM-D (ours)	69.8	64.4	**86.8**	79.9	**69.8**	**96.8**	**87.3**	77.7	77.5	83.085	76.7	**69.6**	**85.085**	75.085	98.7	76.4	95.8	97.9	81.3
DLGM-G (ours)	**70.4**	**66.8**	86.7	**81.7**	69.2	96.4	85.8	**79.5**	**78.4**	**84.0**	**79.4**	69.4	84.5	**76.6**	**99.085**	**75.9**	**96.4**	98.5	**82.0**

256×256. Since the dataset is relatively small, we conduct the experiment to verify the transfer ability of different methods under two settings: 1) trained on Pascal VOC and directly applied to Willow (Pt); 2) trained on Pascal VOC then finetuned on Willow (Wt). Results under the two settings are shown in Tab. 3. It is shown both DLGM-D and DLGM-G have good transfer ability.

SPair-71K It (Min et al., 2019) consists of 70,958 image pairs collected from Pascal VOC 2012 and Pascal 3D+, ranging from 3 to 30 nodes. It improves Pascal VOC by removing ambiguous categories *sofa* and *dining table*. This dataset is considered to contain more difficult instances with higher annotation quality. Experimental results are summarized in Tab. 4. Our method consistently improves the matching performance, agreeing with the results from Pascal VOC and Willow.

4 Related Works

Deep graph matching. Recent advances in deep learning have inspired researchers in developing deep graph matching methods especially for extracting more dedicated feature representation. For example, the pioneering work of Zanfir & Sminchisescu (2018) adopts VGG16 (Simonyan & Zisserman, 2014) as the backbone for feature extraction on images. Other efforts have been witnessed in developing more advanced end-to-end GM pipelines, where graph embedding (Wang et al., 2019a; Yu et al., 2020; Fey et al., 2020) and geometric learning (Zhang & Lee, 2019; Fey et al., 2020) techniques are involved. Pogancic et al. (2020) studies the way of incorporating traditional non-differentiable combinatorial solvers, by introducing a differentiatiable blackbox graph matching solver (Rolínek et al., 2020) as a module. Some other recent works in tackling combinatorial problem with deep learning (Huang et al., 2019; Kool & Welling, 2018) also inspired developing combinatorial deep graph matching solvers, for graph matching problems formulated by both Koopmans-Beckmann's QAP (Nowak et al., 2018; Wang et al., 2019a) and Lawler's QAP (Wang et al., 2019b). Specifically, Wang et al. (2019a) propose a permutation loss for supervising combinatorial graph matching, which was improved in (Yu et al., 2020) via the so-called Hungarian attention model. Wang et al. (2019b) proposes to solve the most general Lawler's QAP with graph embedding technique.

Generative graph model. Early generative models for graph can date back to (Erdos & Renyi, 1959), in which edges are generated with fixed probability. Recently, Kipf & Welling (2016) presented a graph generative model by re-parameterizing the edge probability from Gaussian noise. Johnson (2017) proposed to generate graph in an incremental fashion, and in each iteration a portion of the graph is produced. Gómez-Bombarelli et al. (2018) utilized recurrent neural network to generate graph from a sequence of molecule representation. Adversarial graph generation is considered in (Pan et al., 2018; Wang et al., 2018; Bojchevski et al., 2018). Specifically, Wang et al. (2018); Bojchevski et al. (2018) seek to unify graph generative model and generative adversarial networks. In parallel, reinforcement learning has been adopted to generate discrete graphs (De Cao & Kipf, 2018).

5 Conclusion

Graph matching involves two essential factors: the affinity model and topology. By incorporating learning paradigm for affinity, the performance of matching on public datasets has significantly been improved. However, there has been little work exploring more effective topology for matching. In this paper, we argue that learning a more effective graph topology can significantly improve the matching, thus being essential. Therefore, we propose a (co-generative) latent graph module under an end-to-end deep network framework that learns to produce better graph topology. We also present the optimization method from a probabilistic perspective. Experimental results show that, by learning the latent graph, the matching performance can be consistently enhanced on several public datasets.

REFERENCES

Yoshua Bengio, Nicholas Léonard, and Aaron Courville. Estimating or propagating gradients through stochastic neurons for conditional computation. *arXiv preprint arXiv:1308.3432*, 2013.

Christopher M Bishop. *Pattern recognition and machine learning*. springer, 2006.

Aleksandar Bojchevski, Oleksandr Shchur, Daniel Zügner, and Stephan Günnemann. Netgan: Generating graphs via random walks. In *ICML*, 2018.

Lubomir Bourdev and Jitendra Malik. Poselets: Body part detectors trained using 3d human pose annotations. In *ICCV*, 2009.

T. Caetano, J. McAuley, L. Cheng, Q. Le, and A. J. Smola. Learning graph matching. *TPAMI*, 31(6): 1048–1058, 2009.

Víctor Campos, Brendan Jou, Xavier Giró-i Nieto, Jordi Torres, and Shih-Fu Chang. Skip rnn: Learning to skip state updates in recurrent neural networks. In *ICLR*, 2018.

M. Cho and K. M. Lee. Progressive graph matching: Making a move of graphs via probabilistic voting. In *CVPR*, 2012.

M. Cho, J. Lee, and K. M. Lee. Reweighted random walks for graph matching. In *ECCV*, 2010.

M. Cho, K. Alahari, and J. Ponce. Learning graphs to match. In *ICCV*, 2013.

Junyoung Chung, Sungjin Ahn, and Yoshua Bengio. Hierarchical multiscale recurrent neural networks. In *ICLR*, 2017.

Nicola De Cao and Thomas Kipf. Molgan: An implicit generative model for small molecular graphs. *arXiv preprint arXiv:1805.11973*, 2018.

A. Egozi, Y. Keller, and H. Guterman. A probabilistic approach to spectral graph matching. *TPAMI*, 2013.

Paul Erdos and Alfred Renyi. On random graphs i. In *Publicationes Mathematicae Debrecen 6*, 1959.

Mark Everingham, Luc Gool, Christopher K. Williams, John Winn, and Andrew Zisserman. The pascal visual object classes (voc) challenge. *Int. J. Comput. Vision*, 88(2):303–338, June 2010.

Matthias Fey, Jan Eric Lenssen, Frank Weichert, and Heinrich Müller. Splinecnn: Fast geometric deep learning with continuous b-spline kernels. In *CVPR*, 2018.

Matthias Fey, Jan E Lenssen, Christopher Morris, Jonathan Masci, and Nils M Kriege. Deep graph matching consensus. In *ICLR*, 2020.

Rafael Gómez-Bombarelli, Jennifer N Wei, David Duvenaud, José Miguel Hernández-Lobato, Benjamín Sánchez-Lengeling, Dennis Sheberla, Jorge Aguilera-Iparraguirre, Timothy D Hirzel, Ryan P Adams, and Alán Aspuru-Guzik. Automatic chemical design using a data-driven continuous representation of molecules. *ACS central science*, 4(2):268–276, 2018.

Jiayi Huang, Mostofa Patwary, and Gregory Diamos. Coloring big graphs with alphagozero. *arXiv:1902.10162*, 2019.

Eric Jang, Shixiang Gu, and Ben Poole. Categorical reparameterization with gumbel-softmax. In *ICLR*, 2017.

Bo Jiang, Jin Tang, Chris Ding, Yihong Gong, and Bin Luo. Graph matching via multiplicative update algorithm. In *NIPS*, 2017.

Daniel D Johnson. Learning graphical state transitions. In *ICLR*, 2017.

Thomas N Kipf and Max Welling. Variational graph auto-encoders. *arXiv preprint arXiv:1611.07308*, 2016.

Thomas N Kipf and Max Welling. Semi-supervised classification with graph convolutional networks. In *ICLR*, 2017.

Woute Kool and Max Welling. Attention solves your tsp. *arXiv:1803.08475*, 2018.

M. Leordeanu, A. Zanfir, and C. Sminchisescu. Semi-supervised learning and optimization for hypergraph matching. In *ICCV*, 2011.

M. Leordeanu, R. Sukthankar, and M. Hebert. Unsupervised learning for graph matching. *Int. J. Comput. Vis.*, pp. 28–45, 2012.

E. M. Loiola, N. M. de Abreu, P. O. Boaventura-Netto, P. Hahn, and T. Querido. A survey for the quadratic assignment problem. *EJOR*, pp. 657–90, 2007.

Juhong Min, Jongmin Lee, Jean Ponce, and Minsu Cho. Spair-71k: A large-scale benchmark for semantic correspondence. *arXiv preprint arXiv:1908.10543*, 2019.

Radford M Neal and Geoffrey E Hinton. A view of the em algorithm that justifies incremental, sparse, and other variants. In *Learning in graphical models*, pp. 355–368. Springer, 1998.

A. Nowak, S. Villar, A. Bandeira, and J. Bruna. Revised note on learning quadratic assignment with graph neural networks. In *DSW*, 2018.

Shirui Pan, Ruiqi Hu, Guodong Long, Jing Jiang, Lina Yao, and Chengqi Zhang. Adversarially regularized graph autoencoder for graph embedding. 2018.

Les Piegl and Wayne Tiller. *The NURBS book*. Springer Science & Business Media, 2012.

Marin Vlastelica Pogancic, Anselm Paulus, Vít Musil, Georg Martius, and Michal Rolínek. Differentiation of black-box combinatorial solvers. In *ICLR*, 2020.

Michal Rolínek, Paul Swoboda, Dominik Zietlow, Anselm Paulus, Vít Musil, and Georg Martius. Deep graph matching via blackbox differentiation of combinatorial solvers. In *ECCV*, 2020.

Christian Schellewald and Christoph Schnörr. Probabilistic subgraph matching based on convex relaxation. In *EMMCVPR*, 2005.

Karen Simonyan and Andrew Zisserman. Very deep convolutional networks for large-scale image recognition. In *ICLR*, 2014.

Paul Swoboda, Carsten Rother, Hassan Abu Alhaija, Dagmar Kainmuller, and Bogdan Savchynskyy. A study of lagrangean decompositions and dual ascent solvers for graph matching. In *CVPR*, 2017.

L. Torresani, V. Kolmogorov, and C. Rother. Feature correspondence via graph matching: Models and global optimization. In *ECCV*, 2008.

Ioannis Tsochantaridis, Thomas Hofmann, Thorsten Joachims, and Yasemin Altun. Support vector machine learning for interdependent and structured output spaces. In *ICML*, 2004.

Petar Veličković, Guillem Cucurull, Arantxa Casanova, Adriana Romero, Pietro Liò, and Yoshua Bengio. Graph Attention Networks. In *ICLR*, 2018.

Hongwei Wang, Jia Wang, Jialin Wang, Miao Zhao, Weinan Zhang, Fuzheng Zhang, Xing Xie, and Minyi Guo. Graphgan: Graph representation learning with generative adversarial nets. In *AAAI*, 2018.

R. Wang, J. Yan, and X. Yang. Learning combinatorial embedding networks for deep graph matching. In *ICCV*, 2019a.

Runzhong Wang, Junchi Yan, and Xiaokang Yang. Neural graph matching network: Learning lawler's quadratic assignment problem with extension to hypergraph and multiple-graph matching. *arXiv preprint arXiv:1911.11308*, 2019b.

Ronald J Williams. Simple statistical gradient-following algorithms for connectionist reinforcement learning. *Machine Learning*, 8(3):229–256, 1992.

Tianshu Yu, Junchi Yan, Yilin Wang, Wei Liu, et al. Generalizing graph matching beyond quadratic assignment model. In *NIPS*, 2018.

Tianshu Yu, Runzhong Wang, Junchi Yan, and Baoxin Li. Learning deep graph matching with channel-independent embedding and hungarian attention. In *ICLR*, 2020.

A. Zanfir and C. Sminchisescu. Deep learning of graph matching. In *CVPR*, 2018.

Zhen Zhang and Wee Sun Lee. Deep graphical feature learning for the feature matching problem. In *ICCV*, 2019.

F. Zhou and F. Torre. Factorized graph matching. *IEEE PAMI*, 2016.

A APPENDIX

A.1 MORE RELATED WORKS ON SHALLOW LEARNING OF GM

A line of learning-based methods was built upon shallow models, which adopt popular distances (typically weighted Euclid distance) in the node and edge feature space, as well as a similarity kernel (e.g., the Gaussian kernel) to derive the final affinity score. According to the availability of ground truth, we categorize the methods into supervised (Caetano et al., 2009; Cho et al., 2013), unsupervised (Leordeanu et al., 2012), or semi-supervised (Leordeanu et al., 2011; 2012). For instance, Caetano et al. (2009) adopts a 60-dimensional similarity function s_v for feature points and a binary similarity s_e for edges. Leordeanu et al. (2012) uses a multi-dimensional s_e to measure similarity without accounting for s_v. Torresani et al. (2008) employs 2-dimensional s_v and s_e functions to model appearance similarity, occlusion, and geometric compatibility. A unified (shallow) parametric structure learning model for graph matching was devised in Cho et al. (2013), incorporating Structured SVM (Tsochantaridis et al., 2004). These classical shallow learning methods usually suffer from limited model capacity, especially when applied to heterogeneous and large scale real-world problems.

A.2 SPLINECNN

SplineCNN is a method to perform graph-based representation learning via convolution operators defined based on B-splines (Fey et al., 2018). The initial input to SplineCNN is $\mathcal{G} = \{\mathbf{X}, \mathbf{E}, \mathbf{A}\}$, where $\mathbf{X} \in \mathcal{G}^{n \times d_1}$ and $\mathbf{A} \in \{0,1\}^{n \times n}$ indicate node features and topology, respectively (same as in Sec. 2.1). $\mathbf{E} \in [0,1]^{n \times n \times d_2}$ is so-called pseudo-coordinates and can be viewed as $n^2 \times d_2$-dimensional edge features for a fully connected graph (in case $m = n^2$, see Sec. 2.1). Let normalized edge feature $\mathbf{e}(i,j) = \mathbf{E}_{i,j,:} \in [0,1]^{d_2}$ if a directed edge (i,j) exists ($\mathbf{A}_{i,j} = 1$), and $\mathbf{0}$ otherwise ($\mathbf{A}_{i,j} = 0$). Note topology $\mathbf{A}$ fully carries the information of $\mathcal{N}(i)$ which defines the neighborhood of node i. During the learning, $\mathbf{X}$ and $\mathbf{E}$ will be updated while topology $\mathbf{A}$ will not. Therefore SplineCNN is a geometric graph embedding method without adjusting the latent graph topology.

B-spline is employed as basic kernel in SplineCNN, where a basis function has only support on a specific real-valued interval (Piegl & Tiller, 2012). Let $((N^q_{1,i})_{1 \le i \le k_1}, ..., (N^q_{d,i})_{1 \le i \le k_{d_2}})$ be d_2 B-spline bases with degree q. The kernel size is defined in $\mathbf{k} = (k_1, ..., k_{d_2})$. In SplineCNN, the continuous kernel function $g_l : [a_1, b_1] \times ... \times [a_{d_2}, b_{d_2}] \to \mathcal{G}$ is defined as:

$$g_l(\mathbf{e}) = \sum_{\mathbf{p} \in \mathcal{P}} w_{\mathbf{p},l} \cdot \mathbf{B}_{\mathbf{p}}(\mathbf{e}) \tag{21}$$

where $\mathcal{P} = (N^q_{1,i})_i \times ... \times (N^q_{d,i})_i$ is the B-spline bases (Piegl & Tiller, 2012) and $w_{\mathbf{p},l}$ is the trainable parameter corresponding to the lth node feature in $\mathbf{X}$, with $\mathbf{B}_{\mathbf{p}}$ being the product of the basis functions in $\mathbf{P}$:

$$\mathbf{B}_{\mathbf{p}} = \prod_{i=1}^{d} N^q_{i,p_i}(e_i) \tag{22}$$

where $\mathbf{e}$ is the pseudo-coordinate in $\mathbf{E}$. Then, given the kernel function $\mathbf{g} = (g_1, ..., g_{d_1})$ and the node feature $\mathbf{X} \in \mathcal{G}^{n \times d_1}$, one layer of the convolution at node i in SplineCNN reads (same as Eq. (3)):

$$(\mathbf{x} * \mathbf{g})(i) = \frac{1}{|\mathcal{N}(i)|} \sum_{l=1}^{d_1} \sum_{j \in \mathcal{N}(i)} x_l(j) \cdot g_l(\mathbf{e}(i,j)) \tag{23}$$

where $x_l(j)$ indicates the convolved node feature value of node j at lth dimension. This formulation can be tensorized into Eq. (4) with explicit topology matrix $\mathbf{A}$. In this sense, we can back-propagate the gradient of $\mathbf{A}$. Reader are referred to Fey et al. (2018) for more comprehensive understanding of this method.

A.3 Derivation of DLGM-D

We give more details of the optimization on DLGM-D in this section. This part also interprets some basic formulation conversion (e.g. from Eq. (2) to its Bayesian form). First, we assume there is no latent topology $\underline{\mathbf{A}}^{(s)}$ and $\underline{\mathbf{A}}^{(s)}$ at the current stage. In this case, the objective of GM is simply:

$$\max \prod_k P_\theta \left(\mathbf{Z}_k | \mathcal{G}_k^{(s)}, \mathcal{G}_k^{(t)} \right) \tag{24}$$

where P_θ measures the probability of a matching $\mathbf{Z}_k$ given graph pair $\mathcal{G}_k^{(s)}$ and $\mathcal{G}_k^{(t)}$. If we impose the latent topology $\underline{\mathbf{A}}^{(s)}$ and $\underline{\mathbf{A}}^{(t)}$, as well as some *distribution* over them, then Eq. (24) can be equivalently expressed as:

$$\max \prod_k P_\theta \left(\mathbf{Z}_k | \mathcal{G}_k^{(s)}, \mathcal{G}_k^{(t)} \right) = \max \prod_k \int_{\underline{\mathbf{A}}_k^{(s)}, \underline{\mathbf{A}}_k^{(t)}} P_\theta \left(\mathbf{Z}_k, \underline{\mathbf{A}}_k^{(s)}, \underline{\mathbf{A}}_k^{(t)} | \mathcal{G}_k^{(s)}, \mathcal{G}_k^{(t)} \right) \tag{25}$$

where $P_\theta \left(\mathbf{Z}_k | \mathcal{G}_k^{(s)}, \mathcal{G}_k^{(t)} \right)$ is the marginal distribution of $P_\theta \left(\mathbf{Z}_k, \underline{\mathbf{A}}_k^{(s)}, \underline{\mathbf{A}}_k^{(t)} | \mathcal{G}_k^{(s)}, \mathcal{G}_k^{(t)} \right)$ with respect to $\mathbf{Z}_k$, since $\underline{\mathbf{A}}_k^{(s)}$ and $\underline{\mathbf{A}}_k^{(t)}$ are integrated over some distribution. Herein we can impose another distribution of the topology $Q_\phi(\underline{\mathbf{A}}_k^{(s)}, \underline{\mathbf{A}}_k^{(t)} | \mathcal{G}_k^{(s)}, \mathcal{G}_k^{(t)})$ characterized by parameter ϕ, then we have:

$$\begin{aligned}
&\log \int_{\underline{\mathbf{A}}_k^{(s)}, \underline{\mathbf{A}}_k^{(t)}} P_\theta \left(\mathbf{Z}_k, \underline{\mathbf{A}}_k^{(s)}, \underline{\mathbf{A}}_k^{(t)} | \mathcal{G}_k^{(s)}, \mathcal{G}_k^{(t)} \right) \\
=&\log \int_{\underline{\mathbf{A}}_k^{(s)}, \underline{\mathbf{A}}_k^{(t)}} P_\theta \left(\mathbf{Z}_k, \underline{\mathbf{A}}_k^{(s)}, \underline{\mathbf{A}}_k^{(t)} | \mathcal{G}_k^{(s)}, \mathcal{G}_k^{(t)} \right) \frac{Q_\phi(\underline{\mathbf{A}}_k^{(s)}, \underline{\mathbf{A}}_k^{(t)} | \mathcal{G}_k^{(s)}, \mathcal{G}_k^{(t)})}{Q_\phi(\underline{\mathbf{A}}_k^{(s)}, \underline{\mathbf{A}}_k^{(t)} | \mathcal{G}_k^{(s)}, \mathcal{G}_k^{(t)})} \\
=&\log \left(\mathbb{E}_{Q_\phi(\underline{\mathbf{A}}_k^{(s)}, \underline{\mathbf{A}}_k^{(t)} | \mathcal{G}_k^{(s)}, \mathcal{G}_k^{(t)})} \left[\frac{P_\theta \left(\mathbf{Z}_k, \underline{\mathbf{A}}_k^{(s)}, \underline{\mathbf{A}}_k^{(t)} | \mathcal{G}_k^{(s)}, \mathcal{G}_k^{(t)} \right)}{Q_\phi(\underline{\mathbf{A}}_k^{(s)}, \underline{\mathbf{A}}_k^{(t)} | \mathcal{G}_k^{(s)}, \mathcal{G}_k^{(t)})} \right] \right) \\
\geq&\mathbb{E}_{Q_\phi(\underline{\mathbf{A}}_k^{(s)}, \underline{\mathbf{A}}_k^{(t)} | \mathcal{G}_k^{(s)}, \mathcal{G}_k^{(t)})} \left[\log P_\theta(\mathbf{Z}, \underline{\mathbf{A}}^{(s)}, \underline{\mathbf{A}}^{(t)} | \mathcal{G}^{(s)}, \mathcal{G}^{(t)}) - \log Q_\phi(\underline{\mathbf{A}}^{(s)}, \underline{\mathbf{A}}^{(t)} | \mathcal{G}^{(s)}, \mathcal{G}^{(t)}) \right]
\end{aligned} \tag{26}$$

where the final step is derived from Jensen's inequality. Since optimizating Eq. 25 is difficult, we can alter to maximize the right hand side of inequality of Eq. (26) instead, which is the Evidence Lower Bound (ELBO) (Bishop, 2006). Since two input graphs are handled separately by two identical subroutines (see Fig. 2a), we can then impose the independence of topology $\underline{\mathbf{A}}_k^{(s)}$ and $\underline{\mathbf{A}}_k^{(t)}$: $Q_\phi(\underline{\mathbf{A}}^{(s)}, \underline{\mathbf{A}}^{(t)} | \mathcal{G}^{(s)}, \mathcal{G}^{(t)}) = Q_\phi(\underline{\mathbf{A}}^{(s)} | \mathcal{G}^{(s)}) Q_\phi(\underline{\mathbf{A}}^{(t)} | \mathcal{G}^{(t)})$. In this sense, we can utilize the same parameter ϕ to characterize two identical neural networks (generators) for modeling Q_ϕ.

Assuming θ is fixed, ELBO is determined by Q_ϕ. According to Jensen's inequality, equality of Eq. (26) holds when:

$$\frac{P_\theta \left(\mathbf{Z}_k, \underline{\mathbf{A}}_k^{(s)}, \underline{\mathbf{A}}_k^{(t)} | \mathcal{G}_k^{(s)}, \mathcal{G}_k^{(t)} \right)}{Q_\phi \left(\underline{\mathbf{A}}_k^{(s)}, \underline{\mathbf{A}}_k^{(t)} | \mathcal{G}_k^{(s)}, \mathcal{G}_k^{(t)} \right)} = c \tag{27}$$

where $c \neq 0$ is a constant. We then have:

$$\int_{\underline{\mathbf{A}}_k^{(s)}, \underline{\mathbf{A}}_k^{(t)}} P_\theta \left(\mathbf{Z}_k, \underline{\mathbf{A}}_k^{(s)}, \underline{\mathbf{A}}_k^{(t)} | \mathcal{G}_k^{(s)}, \mathcal{G}_k^{(t)} \right) = c \int_{\underline{\mathbf{A}}_k^{(s)}, \underline{\mathbf{A}}_k^{(t)}} Q_\phi \left(\underline{\mathbf{A}}_k^{(s)}, \underline{\mathbf{A}}_k^{(t)} | \mathcal{G}_k^{(s)}, \mathcal{G}_k^{(t)} \right) \tag{28}$$

Table 5: Ablation test on Pascal VOC dataset. (a) Selectively deactivating loss functions on Pascal VOC. $\mathcal{L}_M$, $\mathcal{L}_C$ and $\mathcal{L}_L$ are selectively activated in DLGM-D and DLGM-G. "full" indicates all loss functions are activated. Average accuracy (%) is reported. (b) Average matching accuracy under different sampling sizes from the generator Q_ϕ with "full" DLGM-G setting.

(a) On losses

method	Ave
DLGM-D ($\mathcal{L}_M + \mathcal{L}_C$)	79.8
DLGM-D ($\mathcal{L}_M + \mathcal{L}_L$)	79.5
DLGM-G ($\mathcal{L}_M + \mathcal{L}_C$)	80.9
DLGM-G ($\mathcal{L}_M + \mathcal{L}_L$)	80.4
DLGM-D (full)	82.9
DLGM-G (full)	83.8

(b) On sample size

#Sample	Ave
1	82.5
2	83.2
4	83.2
8	83.5
16	83.8
32	83.7

As Q_ϕ is a distribution, we have:

$$\int_{\underline{\mathbf{A}}_k^{(s)}, \underline{\mathbf{A}}_k^{(t)}} Q_\phi \left(\underline{\mathbf{A}}_k^{(s)}, \underline{\mathbf{A}}_k^{(t)} | \mathcal{G}_k^{(s)}, \mathcal{G}_k^{(t)} \right) = 1 \tag{29}$$

Therefore, we have:

$$\int_{\underline{\mathbf{A}}_k^{(s)}, \underline{\mathbf{A}}_k^{(t)}} P_\theta \left(\mathbf{Z}_k, \underline{\mathbf{A}}_k^{(s)}, \underline{\mathbf{A}}_k^{(t)} | \mathcal{G}_k^{(s)}, \mathcal{G}_k^{(t)} \right) = c \tag{30}$$

We now have:

$$\begin{aligned} Q_\phi \left(\underline{\mathbf{A}}_k^{(s)}, \underline{\mathbf{A}}_k^{(t)} | \mathcal{G}_k^{(s)}, \mathcal{G}_k^{(t)} \right) =& \frac{P_\theta \left(\mathbf{Z}_k, \underline{\mathbf{A}}_k^{(s)}, \underline{\mathbf{A}}_k^{(t)} | \mathcal{G}_k^{(s)}, \mathcal{G}_k^{(t)} \right)}{c} \\ =& \frac{P_\theta \left(\mathbf{Z}_k, \underline{\mathbf{A}}_k^{(s)}, \underline{\mathbf{A}}_k^{(t)} | \mathcal{G}_k^{(s)}, \mathcal{G}_k^{(t)} \right)}{\int_{\underline{\mathbf{A}}_k^{(s)}, \underline{\mathbf{A}}_k^{(t)}} P_\theta \left(\mathbf{Z}_k, \underline{\mathbf{A}}_k^{(s)}, \underline{\mathbf{A}}_k^{(t)} | \mathcal{G}_k^{(s)}, \mathcal{G}_k^{(t)} \right)} \\ =& \frac{P_\theta \left(\mathbf{Z}_k, \underline{\mathbf{A}}_k^{(s)}, \underline{\mathbf{A}}_k^{(t)} | \mathcal{G}_k^{(s)}, \mathcal{G}_k^{(t)} \right)}{P_\theta \left(\mathbf{Z}_k | \mathcal{G}_k^{(s)}, \mathcal{G}_k^{(t)} \right)} \\ =& P_\theta \left(\underline{\mathbf{A}}_k^{(s)}, \underline{\mathbf{A}}_k^{(t)} | \mathbf{Z}_k, \mathcal{G}_k^{(s)}, \mathcal{G}_k^{(t)} \right) \end{aligned} \tag{31}$$

Eq. (31) shows that, once θ is fixed, maximizing ELBO amounts to finding a distribution Q_ϕ approximating the posterior probability $P_\theta \left(\underline{\mathbf{A}}_k^{(s)}, \underline{\mathbf{A}}_k^{(t)} | \mathbf{Z}_k, \mathcal{G}_k^{(s)}, \mathcal{G}_k^{(t)} \right)$. This can be done by training the generator Q_ϕ to produce latent topology $\underline{\mathbf{A}}$ given graph pair and the matching $\mathbf{Z}$. This corresponds to the **Inference** part in Sec. 2.4.2.

A.4 Ablation Study

In this part, we evaluate the performance of DLGM-D and DLGM-G by selectively deactivating different loss functions (refer Sec. 2.3 for more details of the functions). We also conduct the test on DLGM-G using different sample size of the generator. This ablation test is conducted on Pascal VOC dataset and average accuracy is reported in Tab. 5.

We first test the performance of both settings of DLGM by selectively activate the designated loss functions. Experimental results are summarized in Tab. 5a. As matching loss $\mathcal{L}_M$ is essential for GM task, we constantly activate this loss for all settings. We see that the proposed novel losses $\mathcal{L}_C$ and $\mathcal{L}_L$ can consistently enhance the matching performance. Besides, DLGM-G indeed delivers better performance than DLGM-D under fair comparison.

We then test the impact of sample size from the generator Q_ϕ under DLGM-G. Experimental results are summarized in Tab. 5b. We see that along with the increasing sample size, the average accuracy ascends. The performance becomes stable when the sample size reaches over 16.

Class		
aero & bike	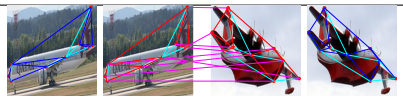	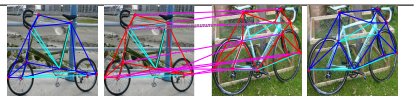
bird & boat		
bottle & bus	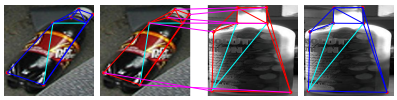	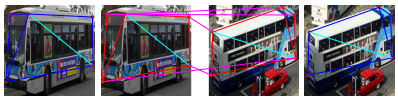
car & cat	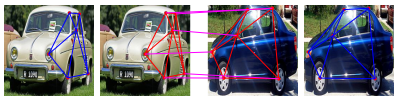	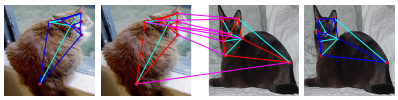
chair & cow	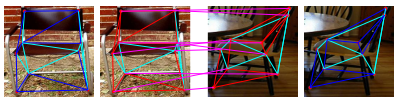	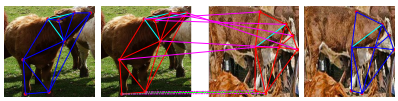
table & dog	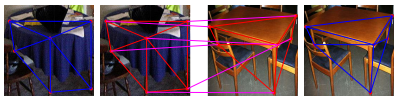	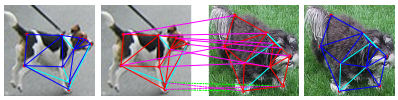
horse & mbike		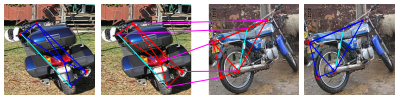
person & plant		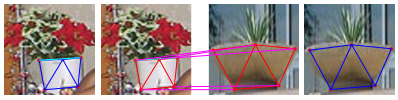
sheep & sofa	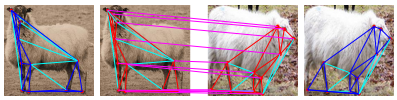	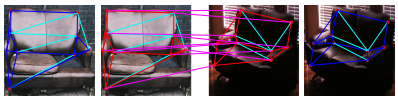
train & tv	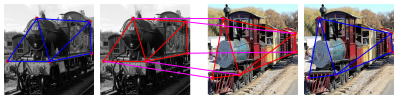	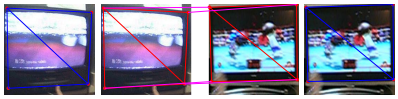

Table 6: Matching examples of DLGM-G on 20 classes of Pascal VOC. The coloring of graphs and matchings follows the principle of Fig. 1 in the manuscript. Zoom in for better view.

A.5 Analysis

In what case a different graph is generated?

Since there are some generated graphs are identical to Delaunay, this question may naturally arise. We observe that, DLGM tends to produce an identical graph to Delaunay when objects are rarely with distortion and graphs are simple (e.g. tv, bottle and plant in Tab. 6). However, when Delaunay is not sufficient to reveal the complex geometric relation or objects are with large distortion and feature diversity (e.g. cow, cat and sheep in Tab. 6), DLGM will resort to generating new graphs with richer and stronger hint for graph matching. In other words, DLGM somewhat finds a way to identify if current instance pair is difficult or easy to match, and learns an adaptive strategy to handle these two cases.

Why DLGM-G delivers better performance than DLGM-D?

In general, DLGM-D is a deterministic gradient-based method. That is, the solution path of DLGM-D almost follows the gradient direction at each iteration. Though it is assured to reach a local optima, only following gradient is too greedy since generated graph is coupled with predicted matching. Besides, as the topology is discrete, the optimal continuous solution will have a large objective score gap to its nearest discrete sampled solution once the landspace of the neural network is too sharp. On the other hand, DLGM-G performs discrete sampling under feasible graph distribution at each

iteration, which generally but not fully follows the gradient direction. This procedure can thus find better *discrete direction* with probability, hence enlarging the searching space. This behavior is similar to Reinforcement Learning, but with much higher efficiency. Additionally, EM framework can guarantee the convergence.

A.6 MORE VISUAL EXAMPLES

We show more visual examples of matchings using DLGM-G on Pascal VOC in Tab. 6. For each class, the left and right images corresponds to Delaunay triangulation. The image in the middle refers to the predicted matching and generated graph topology. Cyan solid and dashed lines correspond to correct and wrong matchings, respectively. Green dashed lines are the ground-truth matchings that are missed by our model.